Full-potential KKR calculations for metals and semiconductors

M. Asato
Graduate School of Electronic Science and Technology, Shizuoka University, Hamamatsu 432-8011, Japan

A. Settels
Institut für Festkörperforschung, Forschungszentrum Jülich, D-52425 Jülich, Germany

T. Hoshino and T. Asada
Department of Applied Physics, Faculty of Engineering, Shizuoka University, Hamamatsu 432-8561, Japan

S. Blügel, R. Zeller, and P. H. Dederichs
Institut für Festkörperforschung, Forschungszentrum Jülich, D-52425 Jülich, Germany
(Received 9 February 1999)

We present systematic total energy calculations for metals (Al, Fe, Ni, Cu, Rh, Pd, and Ag) and semiconductors (C, Si, Ge, GaAs, InSb, ZnSe, and CdTe), based on the all-electron full-potential (FP) Korringa-Kohn-Rostoker Green's-function method, using density-functional theory. We show that the calculated lattice parameters and bulk moduli are in excellent agreement with calculated results obtained by other FP methods, in particular, the full-potential linear augmented-plane-wave method. We also investigate the difference between the local-spin-density approximation (LSDA) and the generalized-gradient approximation (GGA) of Perdew and Wang (PW91), and find that the GGA corrects the deficiencies of the LSDA for metals, i.e., the underestimation of equilibrium lattice parameters and the overestimation of bulk moduli. On the other hand, for semiconductors the GGA gives no significant improvement over the LSDA. We also discuss that a perturbative GGA treatment based on FP-LSDA spin densities gives very accurate total energies. Further, we demonstrate that the accuracy of structural properties obtained by FP-LSDA and FP-GGA calculations can also be achieved in the calculations with spherical potentials, provided that the full spin densities are calculated and all Coulomb and exchange integrals over the Wigner-Seitz cell, occurring in the double-counting contributions of the total energy, are correctly evaluated. [S0163-1829(99)15331-1]

I. INTRODUCTION

The Korringa-Kohn-Rostoker (KKR) method of band-structure calculations was introduced over 50 years ago by Korringa[1] and some years later by Kohn and Rostoker.[2] A characteristic feature of this method is the use of multiple scattering theory, which leads to a beautiful separation of potential and structural properties. As a disadvantage, the method is complicated and demanding from a numerical point of view and as a band-structure method it was therefore soon overtaken by the more efficient linearized methods, such as the linearized muffin-tin-orbital method[3] (LMTO) and the linearized augmented-plane-wave method (LAPW).[4] In the past two decades, the method experienced a revival as a Green's-function method, to which the advantages of linearization no longer apply. Due to the complex energy integration, Green's-function (GF) methods, in particular the KKR-GF method, are computationally very efficient and are able to solve the geometry problem of an impurity in the bulk[5] or on a clean surface[6] without replacing it by an ersatz geometry such as a finite cluster or a supercell. Moreover, the availability of the Green's function allows application to linear-response problems, to disordered alloys by using, e.g., the coherent potential approximation (CPA), and to transport problems.[7]

A limitation of the original KKR method is the restriction to central potentials of muffin-tin or atomic-sphere form. The extension of the KKR method into a full-potential scheme has been extensively and controversially discussed in the literature.[8] Now it is generally accepted that this represents no problem in principle and several realizations of full-potential KKR codes exist.[5,9–14] Here we use the implementation of Drittler *et al.*, which has been extensively used in impurity calculations.[5,9–11] It consists of a Wigner-Seitz partitioning of the whole space, thus eliminating the interstitial region from the formalism. All relevant quantities, i.e., charge density, Kohn-Sham potential, and Green's function, are expanded into angular momenta in each cell. A relativistic extension of this full-potential KKR (FPKKR) scheme has recently been presented by Huhne *et al.*[15]

The main aim of the present paper is to demonstrate that this full-potential KKR formalism is very accurate and that the accuracy is comparable to that of the full-potential LAPW (FLAPW) method, which in this respect represents the state of the art in electronic-structure calculations (Sec. III). For this purpose we performed *ab initio* calculations for the equilibrium lattice parameters a and the bulk moduli B of a series of selected metals and semiconductors. As metals we choose the simple metal Al, the noble metals Cu and Ag, the $3d$ ferromagnets Fe and Ni, and $4d$ metals Rh and Pd. In addition, we give results for the elemental semiconductors C, Si, and Ge, the III-V compound semiconductors GaAs and InSb, and the II-VI compound semiconductors ZnSe and CdTe. For a comparison with FLAPW results, two of us (T.A. and S.B.) have performed calculations with the Jülich FLAPW code for the considered metals.

This paper also has, however, some additional aims. First, we examine the recent development of density-functional

theory.[16,17] For this purpose all calculations are performed both in the local-spin-density approximation[18–21] (LSDA) and in the generalized-gradient approximation proposed by Perdew and Wang (PW91-GGA).[22,23] In agreement with other authors,[24] we find for the transition metals, in particular the $3d$ metals, that the underestimation of the lattice parameters and the overestimation of the bulk moduli, being a characteristic result of the LSDA, are corrected very well by the GGA (Sec. III). On the other hand, for semiconductors the GGA gives no significant improvement, since the lattice parameters slightly improve while the bulk moduli become worse (Sec. IV).

Second, we discuss in this paper the accuracy of ''full-charge'' compared to ''full-potential'' calculations.[25,26] The full-charge calculations use a spherical potential. However, the fully anisotropic charge density is calculated and used in the determination of the spherical potential as well as in the evaluation of the Coulomb and exchange correction contribution to the total energies. In general, we find that for the total energies practically the same accuracy can be obtained as in full-potential calculations, but with a considerably reduced effort (Sec. V).

Finally we discuss a perturbative treatment of the gradient corrections (GC), where the GGA total energy functional is evaluated with self-consistent LSDA spin densities as input. This avoids the slowly converging self-consistency iterations for the GGA Kohn-Sham equations, and yields, as we will show, the same accuracy of the total energies as a fully self-consistent GGA treatment does (Sec. VI). Section VII summarizes the main results.

II. METHOD OF CALCULATIONS

All the calculations presented here are based on density-functional theory[16,17] in the local-spin-density approximation[18–21] (LSDA) and the generalized-gradient approximation (PW91-GGA) proposed by Perdew and Wang.[22,23] To solve the Kohn-Sham equations, we use multiple-scattering theory in the form of the KKR Green's-function method for full potentials, developed by Drittler *et al.*[5,9–11] This method is shortly sketched in the following.

In a multiple-scattering treatment, one represents the crystal potential as a sum of nonoverlapping cellular potentials which fill up the space completely. The Green's function $G(\mathbf{r}+\mathbf{R}^n,\mathbf{r}'+\mathbf{R}^{n'})$ of this system can be written in a cell-centered representation as[5,9–11]

$$G(\mathbf{r}+\mathbf{R}^n,\mathbf{r}'+\mathbf{R}^{n'};E)=\sqrt{E}\,\delta_{nn'}\sum_L H_L^n(\mathbf{r}_>;E)R_L^n(\mathbf{r}_<;E) + \sum_{LL'} R_L^n(\mathbf{r};E)G_{LL'}^{nn'}(E)R_{L'}^{n'}(\mathbf{r}';E). \tag{1}$$

The vectors $\mathbf{r}$ and $\mathbf{r}'$ are restricted to the Wigner-Seitz cells around the atomic positions $\mathbf{R}^n$ and $\mathbf{R}^{n'}$, $\mathbf{r}_>(\mathbf{r}_<)$ denotes the larger (smaller) of the vectors $\mathbf{r}$ and $\mathbf{r}'$ in absolute value, and $L=(l,m)$ denotes angular momentum numbers. $R_L^n(\mathbf{r},E)$ is the solution of the single-potential-scattering problem for a spherical wave $j_l(\sqrt{E}r)Y_L(\hat{\mathbf{r}})$ of angular momentum L incident on the general potential $V^n(\mathbf{r})$ of cell n,[27]

$$R_L^n(\mathbf{r};E)=j_l(\sqrt{E}r)Y_L(\hat{\mathbf{r}}) + \int d\mathbf{r}'\,g(\mathbf{r},\mathbf{r}';E)V^n(\mathbf{r}')R_L^n(\mathbf{r}';E). \tag{2}$$

Here $j_l(x)$ is a spherical Bessel function and $Y_L(\hat{\mathbf{r}})$ is a spherical harmonic, while $g(\mathbf{r},\mathbf{r}';E)$ is the Green's function for free space given by

$$g(\mathbf{r},\mathbf{r}';E)=-\frac{\exp(i\sqrt{E}|\mathbf{r}-\mathbf{r}'|)}{4\pi|\mathbf{r}-\mathbf{r}'|}. \tag{3}$$

The structural Green's-function matrix $G_{LL'}^{nn'}(E)$ contains all the information of the multiple scattering and can be related to the analytically known structural matrix $g_{LL'}^{nn'}(E)$ of the free-electron Green's function by a Dyson equation,

$$G_{LL'}^{nn'}(E)=g_{LL'}^{nn'}(E)+\sum_{n''}\sum_{L''L'''} g_{LL''}^{nn''}(E)t_{L''L'''}^{n''}(E)G_{L'''L'}^{n''n'}(E). \tag{4}$$

Here $t_{L''L'''}^{n''}(E)$ are the single-scattering t matrices to be obtained from the potential $V^{n''}(\mathbf{r})$ inside the atomic cell centered at the position $\mathbf{R}^{n''}$. Only for spherical potentials is this t matrix diagonal in the angular momentum indices.

For a general potential, the solution of Eq. (2) is nontrivial. We expand the wave function $R_L^n(\mathbf{r},E)$ and the single-cell potential $V^n(\mathbf{r})$ into spherical harmonics.[5,9] By dropping the site indices n we write the expansion as

$$R_L(\mathbf{r},E)=\sum_{L'} R_{L'L}(r,E)Y_{L'}(\hat{\mathbf{r}}), \quad V(\mathbf{r})=\sum_L V_L(r)Y_L(\hat{\mathbf{r}}). \tag{5}$$

The nonspherical components $V_L(\mathbf{r})$ for $l\neq 0$ lead to a coupled set of radial equations for the different partial waves $R_{L'L}$. These equations are conveniently solved in two steps. We first calculate the solutions $R_l^0(r;E)Y_L(\hat{\mathbf{r}})$ for the radial symmetric potential $V_{l=0}(r)$, which dominates the behavior. We then solve the radial integral equation for the wave functions $R_{L'L}$,

$$R_{L'L}(r,E)=R_L^0(r,E)\,\delta_{L'L}+\int_0^{R_C} dr'\,r'^2 g_{l'}^0(r,r';E) \times\sum_{L''}\Delta v_{L'L''}(r')R_{L''L}(r';E), \tag{6}$$

where $g_{l'}^0(r,r';E)$ is the radial Green's function for the isotropic potential $V_{l=0}(r)$ and the integration is executed only up to the circumscribed radius R_C of the Wigner-Seitz cell. $\Delta v_{LL'}(r)$ is directly related to the small and purely anisotropic part of the potential

$$\Delta v_{LL'}(r)=\sum_{L''\neq 0} C_{LL'L''}V_{L''}(r), \tag{7}$$

where the C's are Gaunt coefficients. Due to the smallness of $\Delta v_{LL'}(r)$, we solve Eq. (6) by iteration. Usually the second Born approximation with respect to $\Delta v_{LL'}(r)$ is completely sufficient to obtain reliable densities. Moreover, the aniso-

tropic potentials $\Delta v_{LL'}(r)$ are only important in the outer regions of the cell, say for r larger than half the muffin-tin radius. Thus Eq. (6) must be solved only on a relatively small number of mesh points, since in the core region, where many more mesh points are needed, the potential is quite isotropic. Both aspects, the second Born approximations and the restriction of the number of mesh points, reduce the computing time considerably, but these approximations can also be easily avoided.

The maximum angular momentum used in the expansion of the wave functions and the Green's functions is set to $l_{\max}=4$, which according to our experience is sufficient to obtain well-converged results.[28] This conclusion is also confirmed from the comparison of the present calculations with the FLAPW results discussed in Sec. III. Analogously, $V(\mathbf{r})$ of Eq. (5) and the electron density $n(\mathbf{r})$ include all angular momentum coefficients up to $2l_{\max}=8$. In solving the Kohn-Sham and Poisson equations, the exact form of the Wigner-Seitz cell is described by a shape function $\Theta(\mathbf{r})$, which equals 1 inside the Wigner-Seitz cell and zero otherwise. The shape function is expanded into spherical harmonics,

$$\Theta(\mathbf{r})=\sum_L \Theta_L(r)Y_L(\hat{\mathbf{r}}). \tag{8}$$

The expansion coefficients $\Theta_L(r)$ are calculated using the algorithm of Stefanou *et al.*[29,30] Only shape function coefficients up to $4l_{\max}=16$ are needed in the present calculations.

The electron density is calculated from the Green's function by a contour integral in the complex energy plane.[31] For the occupation function we use a Fermi-Dirac distribution with a finite temperature of $T=800$ K for metals ($T=450$ K for semiconductors).[32] The contour integral is evaluated with 46 complex energy points in total. The Brillouin zone integrations are performed using 146 k points for the fcc structure and 91 k points for the bcc structure, both of which are in the irreducible Brillouin zone. It is noted that the lattice structure for semiconductors is of zinc-blende type treated with two extra empty spheres, which is also described by a fcc lattice with four basis atoms along the (111) direction. The calculations adopt the scalar relativistic approximation, which becomes important to obtain accurate results for the $4d$ metals.[33]

III. FPKKR RESULTS FOR BULK PROPERTIES OF METALS

We discuss the calculated LSDA and PW91-GGA results for Al, Fe, Ni, Cu, Rh, Pd, and Ag. In the present work we carried out the FPKKR calculations with two prescriptions for the muffin-tin radius: (i) the muffin-tin radius being scaled together with the value of lattice parameter (scaled MT) and (ii) the muffin-tin radius being independent of the value of the lattice parameter (fixed MT).[34] Figure 1 shows the lattice-parameter dependence of the total energies for the above metals, obtained by fixed-MT calculations. The vertical lines show the measured equilibrium lattice parameters.[35] In addition, Table I lists the numerical values for the lattice parameter a and the bulk modulus B, obtained by fitting Murnaghan's equation of state[36] to the calculated total energies. The errors in a and B with respect to experimental data[35] are also shown in Figs. 2(a) and 2(b), respectively. Results obtained by other full-potential methods [full-potential linearized augmented-plane-wave method (FLAPW) and full-potential linear muffin-tin-orbital method[24] (FPLMTO)] as well as the experimental values are also listed in Table I. Although the differences between the calculated results for the two kinds of muffin-tin treatments are very small ($\Delta a \leqslant 0.02$ a.u. and $\Delta B \leqslant 0.04$ Mbar), as seen in Table I, we believe that the fixed-MT results are more accurate than the scaled-MT ones since the numerical errors in the total-energy part due to both the integration and renormalization of inactive core orbitals are eliminated in the fixed-MT treatment, which uses the same mesh points inside the muffin-tin radius. We have also checked that the calculated results do not change for a reasonable variation of a fixed-MT radius ($\sim$0.2 a.u.). The calculated results can be summarized as follows: (i) The FPKKR-LSDA and FPKKR-GGA results, using fixed-MT's, agree very well with FLAPW-LSDA and FLAPW-GGA results, both of which use a fixed-MT procedure ($\Delta a < 0.02$ a.u. and $\Delta B < 0.1$ Mbar); (ii) the FPKKR-LSDA and FPKKR-GGA results, using scaled-MT's, agree very well ($\Delta a < 0.02$ a.u. and $\Delta B < 0.02$ Mbar) with FPLMTO-LSDA and FPLMTO-GGA results, which also used scaled MT's; (iii) the GGA calculations correct the underestimation of a and the overestimation of B due to the LSDA, for all elements in Table I, in particular for Al, Fe, Ni, and Cu.

In case of the LSDA, the FPKKR calculations used the LSDA functional of von Barth and Hedin with the fitting parameters as given by Morruzi, Janak, and Williams (MJW),[19,20] while the FLAPW calculations refer to the LSDA functional of von Barth and Hedin with the fitting parameter of Hedin and Lundqvist (vBH).[18,19] We found that the differences between MJW-LSDA and vBH-LSDA results are very small ($\Delta a < 0.02$ a.u. and $\Delta B < 0.05$ Mbar). Thus the present calculations confirm the well-established effect of the gradient corrections (GC's) to increase a and decrease B, leading to the nice agreement with the experimental results, as seen in Figs. 2(a) and 2(b). The increase of a may be explained by noting that the PW91-GGA functional favors spin-density inhomogeneities. The decrease in B is strongly related to the increase in a.

Finally, we discuss the magnetism for Ni and Fe. Figure 3 shows the lattice parameter dependence of the magnetic moment and the magnetic energy of Fe, obtained by the FP-LSDA and FP-GGA calculations (○,●). For Fe, the magnetic moment does not change due to the GC's, but the spin polarization energy strongly increases by $\sim$0.1 eV, which leads to the prediction of the correct ground-state structure of Fe. This result agrees with the result obtained by FLAPW calculations.[37] However, it is also noted in Fig. 3(a) that, in contrast to the result obtained by the FP calculations, the GGA calculations based on the atomic-sphere-approximation (ASA) (■) show a significant enhancement of the magnetization over the LSDA (□), as has been discussed in Ref. 37. It is also seen in Fig. 3(b) that in the ASA the increase in the spin polarization energy is small ($\sim$0.05 eV), compared with the FP calculations ($\sim$0.1 eV). Thus it may be concluded that the FP calculations are indeed needed in order to investigate the GC effect on the magnetic properties of Fe, which are determined to a large extent by anisotropic spin densities

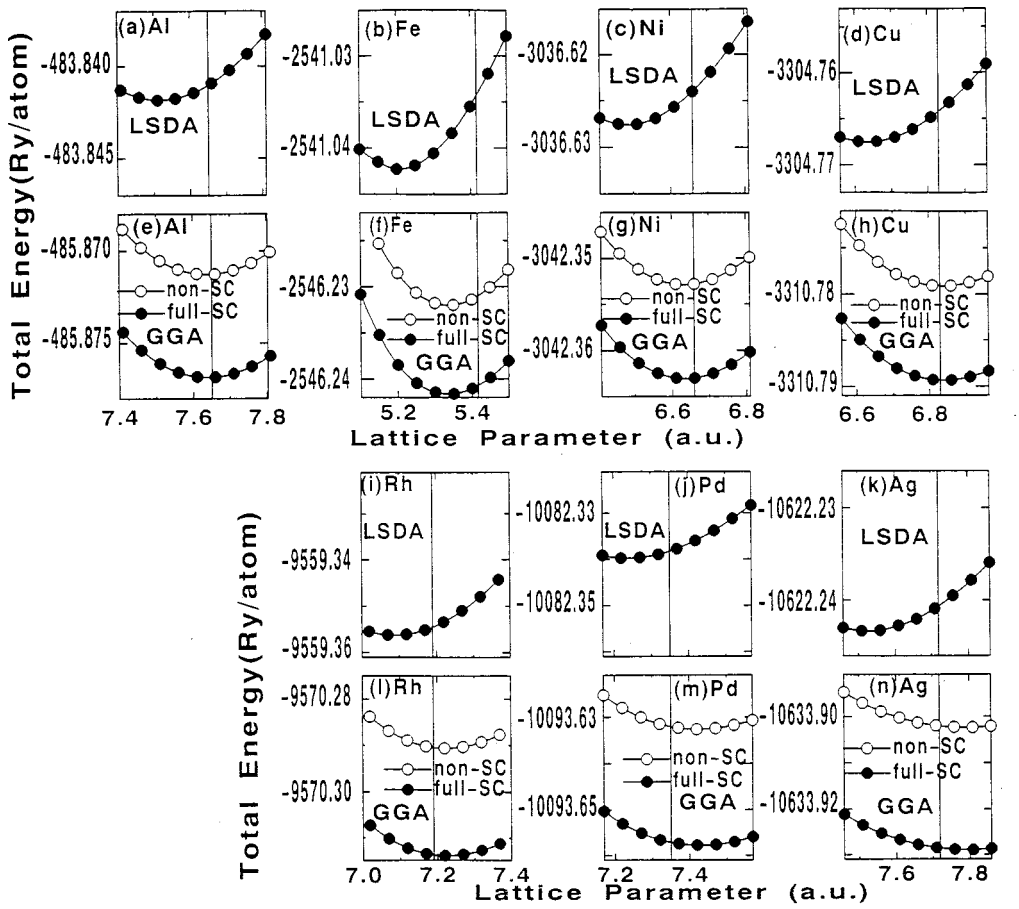

FIG. 1. Structural energy-lattice parameter curves for Al, Fe, Ni, Cu, Rh, Pd, and Ag, obtained by LSDA [(a)–(d), (i)–(k), closed circles] and GGA [(e)–(h), (l)–(n), closed circles]. The non-SC-GGA calculation results are also shown (open circles). See the text (Sec. V) for details.

and their GC part. As seen in Fig. 4, in the case of Ni the FP calculations decrease the magnetic moments and increase the magnetic energies, compared to results of ASA calculation. Contrary to the results for Fe, the GC effect for Ni is small ($\sim$0.01 eV) and almost same in FP and ASA calculations since the anisotropic part of the Ni potential is not large. We also discuss in Sec. VI the fact that, compared with the FP calculated results, the ASA approximation overestimates the lattice parameter for Fe, as discussed in Refs. 37 and 38, but underestimates the lattice parameter of Ni.

IV. FPKKR RESULTS FOR BULK PROPERTIES OF SEMICONDUCTORS

Here we compare the results of the FPKKR calculations for the elemental semiconductors (C, Si, Ge) and compound semiconductors (GaAs, InSb, ZnSe, CdTe), crystallizing in diamond or zinc-blende-type structure, with all-electron FLAPW calculations[39] and experiments.[40] The LSDA calculations were performed with the parametrization of Vosko, Wilk, and Nusair (VWN),[21] contrary to the MJW functional[20] used for metals. We have checked that the differences between the calculated results of VWN-LSDA and MJW-LSDA are very small. The present GGA calculations use the perturbative approach, described in Sec. V, which exploits the variational property of the total energy. Table II shows the results for the equilibrium lattice parameters and bulk moduli calculated in the LSDA and GGA, by using the same fitting process as described in Sec. III.[36] All calculations were performed with fixed muffin-tin radii. Considering the different parameterizations for the exchange-correlation energy functional used in both methods, our LSDA results for the equilibrium lattice parameters and bulk moduli are in good agreement with FLAPW results,[39] as seen in Table II. The FPKKR-GGA results agree very well with the FLAPW-GGA results, both using the PW91-GGA. Contrary to the trend to underestimate the lattice parameters in the LSDA, the GGA calculations overestimate the experimental results[40] for all semiconductors considered here, as can be seen from Fig. 5(a). While the LSDA results for the elemental semiconductors differ less than 1.5% from experimental data, the values for compound semiconductors deviate in a range from 1% to 2.8%. Overall, the lattice parameters with the GGA functional are in better agreement with the experimental data and the deviation is smaller than 1.2% for all cases. On the other hand, the GGA calculations give lower values for the bulk moduli for all elements, as seen in Fig. 5(b). Since for the elemental semiconductors the LSDA already underestimates the experimental data, the GGA treatment makes the result worse. For the compound semiconductors, the LSDA calculations overestimate the experimental bulk moduli, while the GGA calculations underestimate them, such that both calculations show approximately the same deviation from the experiment.

TABLE I. LSDA and PW91-GGA results for equilibrium lattice constant a and bulk modulus B, obtained by the full-potential KKR Green's-function method. The experimental results (Ref. 35) as well as calculated results obtained by other full-potential methods are also shown for a comparison.

	Al	Fe	Ni	Cu	Rh	Pd	Ag
				a (a.u.)			
FPKKR-LSDA (scaled MT)	7.55	5.22	6.48	6.65	7.11	7.27	7.56
FPKKR-LSDA (fixed MT)	7.52	5.20	6.46	6.63	7.09	7.24	7.53
FLAPW-LSDA	7.51	5.18	6.46	6.63	7.09	7.25	7.54
FPLMTO-LSDA[a]					7.11	7.25	
FPKKR-GGA (scaled MT)	7.67	5.37	6.66	6.86	7.26	7.46	7.82
FPKKR-GGA (fixed MT)	7.64	5.34	6.63	6.84	7.22	7.43	7.79
FLAPW-GGA	7.65	5.34	6.64	6.85	7.24	7.45	7.82
FPLMTO-GGA[a]					7.26	7.45	
Experiment	7.65	5.42	6.66	6.84	7.19	7.35	7.72
				B (Mbar)			
FPKKR-LSDA (scaled MT)	0.83	2.41	2.53	1.89	3.15	2.27	1.41
FPKKR-LSDA (fixed MT)	0.82	2.43	2.54	1.88	3.18	2.28	1.39
FLAPW-LSDA	0.85	2.57	2.56	1.90	3.12	2.29	1.41
FPLMTO-LSDA[a]					3.13	2.26	
FPKKR-GGA (scaled MT)	0.73	1.84	1.98	1.42	2.56	1.72	0.96
FPKKR-GGA (fixed MT)	0.73	1.88	2.00	1.38	2.58	1.72	0.98
FLAPW-GGA	0.73	1.86	2.04	1.41	2.54	1.68	0.93
FPLMTO-GGA[a]					2.57	1.71	
Experiment	0.72	1.68	1.86	1.37	2.70	1.81	1.01

[a]Reference 24.

V. PERTURBATIVE GGA CALCULATIONS WITH FP-LSDA SPIN-DENSITIES

In this section we discuss the accuracy of a perturbative treatment of the GC's, which eliminates the need to solve the GGA-Kohn-Sham equations self-consistently.[41] According to the density-functional formalism, there exists a unique energy functional which is variational in the spin density. Hence, if the functional is evaluated with a trial spin density close to the exact ground-state spin density, the error in the total energy is only of second order in the difference between the trial spin density and the exact ground-state spin density. Therefore, we evaluate the GGA total energies by using the self-consistent (SC) -LSDA densities as input. This should

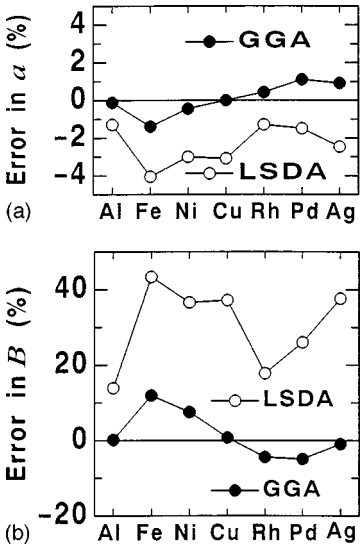

FIG. 2. Errors in calculated equilibrium lattice parameters a (a) and bulk moduli B (b) with respect to experimental data.

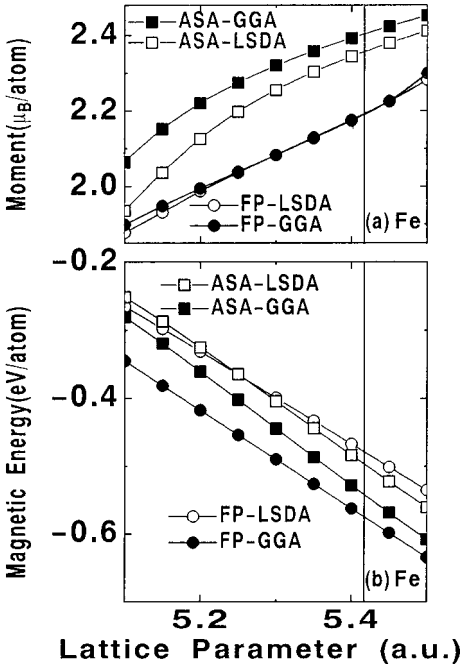

FIG. 3. Lattice parameter dependence of magnetic moment (a) and magnetic energy (b) for Fe.

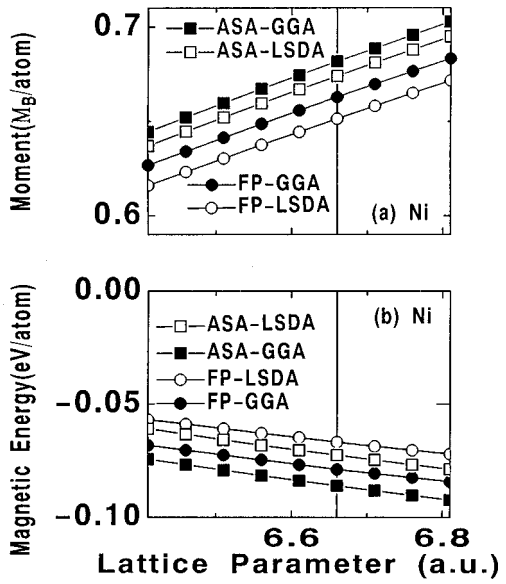

FIG. 4. Lattice parameter dependence of magnetic moment (a) and magnetic energy (b) for Ni.

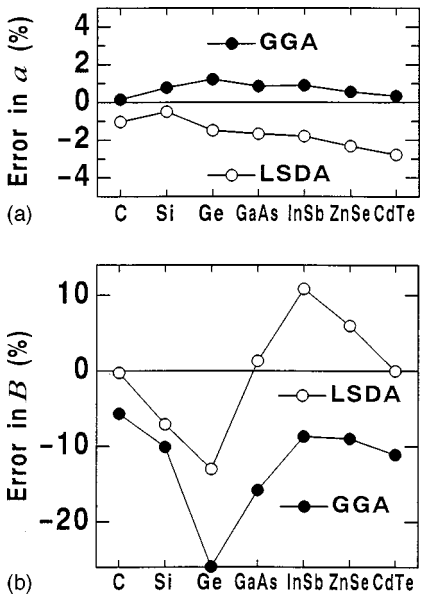

FIG. 5. Errors in calculated equilibrium lattice parameters a (a) and bulk moduli B (b) with respect to experimental data.

be justified since the gradient corrections affect the total energies only slightly, as can be seen from Fig. 1. For example, the total-energy changes due to the GC effect are as small as ~ -2, -5, -6, -6, -11, -11, and -12 Ry for Al, Fe, Ni, Cu, Rh, Pd, and Ag, while the LSDA total energies are ~ -484, -2541, -3037, -3305, -9559, $-10\,082$, and $-10\,622$ Ry. Thus we may expect that the LSDA spin densities are similar to the GGA spin densities. The calculated total energies for Al, Fe, Ni, Cu, Rh, Pd, and Ag, obtained in this way, are also shown in Fig. 1 (○). We can see that the perturbative GGA treatment based on the FP-LSDA spin densities reproduces almost completely the lattice parameter dependence of total energies, although the correct GGA total energies are still slightly lower in energy (by about ~ 0.005 Ry for Al, ~ 0.01 Ry for Fe, Ni, Cu, and ~ 0.02 Ry for Rh, Pd, Ag). The values of a and B, obtained by the perturbative calculations, agree very well with the results obtained by the full self-consistent GGA calculations, as seen in Table III: the errors are as small as $\Delta a \leqslant 0.01$ a.u. and $\Delta B \leqslant 0.05$ Mbar except for Fe. It is also found for Fe that the error for the bulk moduli becomes somewhat large ($\Delta B \sim 0.13$ Mbar) since the nonspherical spin densities, correlated strongly to the GC effect,[37] become important. However, the error is still small. Thus we may conclude that the FP-LSDA spin densities are useful to obtain the accurate lattice constants and bulk moduli by the GGA density functional, thus avoiding a self-consistent evaluation of the GGA spin densities.

TABLE II. LSDA and PW91-GGA results for equilibrium lattice constant a and bulk modulus B, obtained by the full-potential KKR Green's-function method. The experimental results (Ref. 40) as well as calculated results obtained by other full-potential methods are also shown for a comparison.

	C	Si	Ge	GaAs	InSb	ZnSe	CdTe
				a (a.u.)			
FPKKR-LSDA (fixed MT)	6.67	10.21	10.53	10.50	12.02	10.46	11.91
FLAPW-LSDA[a]		10.22	10.63	10.62			
FPKKR-GGA (fixed MT)	6.75	10.34	10.82	10.77	12.35	10.77	12.29
FLAPW-GGA[a]		10.38	10.86	10.84			
Experiment	6.74	10.26	10.69	10.68	12.24	10.71	12.25
				B (Mbar)			
FPKKR-LSDA (fixed MT)	4.41	0.92	0.67	0.77	0.51	0.71	0.45
FLAPW-LSDA[a]		0.96	0.78	0.74			
FPKKR-GGA (fixed MT)	4.17	0.89	0.57	0.64	0.42	0.61	0.40
FLAPW-GGA[a]		0.83	0.61	0.65			
Experiment	4.43	0.99	0.77	0.76	0.46	0.67	0.45

[a]Reference 39.

TABLE III. Equilibrium lattice constant a and bulk modulus B, obtained by perturbative (non-SC) PW91-GGA calculations, are compared to the fully self-consistent FP-PW91-GGA results. The experimental results (Ref. 35) are also given.

	Al	Fe	Ni	Cu	Rh	Pd	Ag
				a (a.u.)			
non-SC-FP-GGA (fixed MT)	7.637	5.337	6.633	6.837	7.223	7.424	7.790
FP-GGA (fixed MT)	7.639	5.335	6.634	6.839	7.224	7.427	7.794
Experiment	7.65	5.42	6.66	6.84	7.19	7.35	7.72
				B (Mbar)			
non-SC-FP-GGA (fixed MT)	0.737	2.018	2.007	1.422	2.622	1.709	0.984
FP-GGA (fixed MT)	0.729	1.877	1.995	1.383	2.576	1.722	0.978
Experiment	0.72	1.68	1.86	1.37	2.70	1.81	1.01

VI. FULL CHARGE-DENSITY (SPIN-DENSITY) VERSUS FULL-POTENTIAL CALCULATIONS

Although FP calculations are very accurate, they are very time-consuming. Therefore, it is worthwhile to ask what kind of accuracy one can obtain in calculations with spherical potentials. This is done in ASA calculations.[25,26] However, here usually three different spherical approximations are made simultaneously: (i) a spherical potential with a cutoff at the Wigner-Seitz radius is used to solve the Kohn-Sham equations (ASA-I), (ii) only the spherical component of the charge densities (or spin densities) is calculated (ASA-II), and (iii) all integrations, e.g., for the Coulomb potential or the Coulomb and exchange energies, are performed over the overlapping Wigner-Seitz sphere in order to calculate the double-counting contribution to the total energy (ASA-III). For the following procedure, the basic idea is to avoid the approximations ASA-II and ASA-III while still retaining the efficiency of a spherical potential calculation. Here we test two such approaches with spherical potentials. In the present ASA approximation (see Table IV), we retain the ASA-I and ASA-III, but generate all angular momentum components of the charge density (up to $2l_{\max}=8$, since all higher components vanish) and use these in the evaluation of the total

TABLE IV. Equilibrium lattice constant a and bulk modulus B, obtained by total-energy calculations with full charge densities which are calculated by use of spherical potentials (ASA and SHP). The experimental results (Ref. 35) as well as the theoretical results obtained by the full charge technique of Vitos, Kollár, and Skriver (Ref. 26) are also shown for a comparison.

	Al	Fe	Ni	Cu	Rh	Pd	Ag
				a (a.u.)			
ASA-LSDA (scaled MT)	7.49	5.26	6.43	6.59	7.04	7.19	7.46
SHP-LSDA (scaled MT)	7.56	5.22	6.49	6.66	7.12	7.27	7.57
SHP-LSDA (fixed MT)	7.51	5.20	6.46	6.63	7.09	7.24	7.53
FP-LSDA (fixed MT)	7.52	5.20	6.46	6.63	7.09	7.24	7.53
SHP-GGA (fixed MT)	7.65	5.33	6.63	6.84	7.23	7.43	7.80
FP-GGA (fixed MT)	7.64	5.34	6.63	6.84	7.22	7.43	7.79
LMTO-ASA-LSDA[a]					7.12	7.24	7.57
LMTO-ASA-GGA[a]					7.26	7.43	7.81
Experiment	7.65	5.42	6.66	6.84	7.19	7.35	7.72
				B (Mbar)			
ASA-LSDA (scaled MT)	0.92	2.24	2.72	2.09	3.46	2.53	1.63
SHP-LSDA (scaled MT)	0.82	2.41	2.52	1.88	3.12	2.25	1.39
SHP-LSDA (fixed MT)	0.80	2.48	2.53	1.86	3.14	2.24	1.37
FP-LSDA (fixed MT)	0.82	2.43	2.54	1.88	3.18	2.28	1.39
SHP-GGA (fixed MT)	0.72	1.93	1.99	1.40	2.57	1.70	0.97
FP-GGA (fixed MT)	0.73	1.88	2.00	1.38	2.58	1.72	0.98
LMTO-ASA-LSDA[a]					3.18	2.24	1.44
LMTO-ASA-GGA[a]					2.59	1.74	0.94
Experiment	0.72	1.68	1.86	1.37	2.70	1.81	1.01

[a]Reference 26.

energy, while performing all integrations over the Wigner-Seitz sphere. The resulting ASA-LSDA data in Table IV are not very good and represent no significant improvement over the usual simple ASA,[42] using the three approximations mentioned above. This is a consequence of the cubic symmetry of the considered systems, for which the higher charge multipoles play only a minor role, since the first nonvanishing multipole occurs for $l=4$.

The second approach avoids both the ASA-II and ASA-III and uses the spherical part, i.e., the $l=0$ component of the anisotropic FP to generate the full charge density, called the shape-potential (SHP). In this approach the exact form of the Wigner-Seitz cell is described by shape functions and all integrals for the Coulomb and exchange-correlation energies are evaluated exactly.[43] From the calculated data listed in Table IV, one finds that the SHP calculations reproduce almost completely the FP results, both for the LSDA as well as the GGA, which is in contrast to the usual claim in the literature that accurate GGA results can only be obtained by a FP treatment. The only exception is Fe, where the FP treatment may be important not only for the local moment and the spin polarization energy, but also for the bulk modulus, as mentioned in the preceding section.

We may conclude from the results of Table IV that also with spherical potentials highly accurate total energies can be obtained, provided that the full charge density (or spin density) is evaluated and integrals over the Wigner-Seitz cell are calculated correctly using shape functions. For the cubic systems considered here, the correct integration gives the biggest improvement, since only relatively high multipole components of the charge density with $l=4$, 6, and 8 exist. On the other hand, for systems with lower symmetry, e.g., a vacancy or a surface, the dipolar or quadrupolar components of the spin density play a decisive role. For instance, for the vacancy in Cu we found previously by using the LSDA calculations that a simple-ASA calculation, using the three approximations ASA-I, ASA-II, and ASA-III, yields a ridiculous vacancy formation energy of about 2.85 eV, more than double the experimental value, while the inclusion of the charge multipoles reduces this value by about 1.2 eV.[44] The inclusion of the shape function (exact treatment for the Wigner-Seitz cell) lowers this value by 0.13 eV, while the FP treatment leads to another lowering of 0.1 eV, finally yielding a vacancy formation energy of 1.41 eV, in good agreement with the experiment.[44]

Our results are in good agreement with the conclusions of Vitos *et al.*[26] that their full charge-density scheme based on LMTO-ASA calculations reproduces very well the results obtained by a FP treatment. Their data for Rb, Pd, and Ag are also included in Table IV, both for the LSDA and GGA. The agreement with our results is good, in particular if we compare with ''scaled-MT'' calculations (using a radial mesh scaling with the lattice constant). As noted earlier, however, calculations with fixed MT's yield a higher accuracy.

In summarizing, we conclude that in most cases a time-consuming FP calculation can be substituted by a more efficient full charge-density (spin-density) calculation. However, this is only correct for the total energy. For instance, a calculation for forces by the Hellmann-Feyman theorem requires a highly accurate calculation of the dipolar charge distribution which can only be obtained if these components are calculated self-consistently, i.e., in a FP treatment.[44] Analogously electric field gradients are determined by the quadrupolar charge components,[45] which usually also require a FP treatment.

VII. SUMMARY AND CONCLUSION

We have shown that the present FPKKR method as a band-structure method gives lattice parameters and bulk moduli with the same accuracy as that of the FLAPW method, which is considered to be the most accurate method available. If identical LSDA or GGA density functionals are used in the calculations, the differences of the FPKKR and FLAPW results are as small as $\sim$0.01 a.u. ($\sim$0.05 Mbar) for a lattice parameter (bulk modulus) of Al, Fe, Ni, Cu, Rh, Pd, and Ag, as seen in Table I.

Second, we have shown that the PW91-GGA corrects the deficiencies of the LSDA for these metals, as seen in Figs. 2(a) and 2(b). The LSDA underestimates lattice parameters (bulk moduli) of the metals by 1–4 % (15–45 %), while the GGA reduces the errors to less than 1% (10%). The gradient-correction (GC) effect over the LSDA is especially significant for the magnetic systems with large anisotropic potentials. For Fe the increase in the magnetic energy is as large as $\sim$0.1 eV, leading to the prediction of the exact ground-state structure and therefore providing an important improvement over the LSDA. It has also been shown that this significant increase cannot be obtained by spherical-potential calculations since the GC effect favors very much the nonsphericity of the potential; the increase in the magnetic energy due to the GC effect becomes smaller than 0.05 eV if the ASA is used in the calculations, as seen in Fig. 3

For semiconductors, such as C, Si, Ge, GaAs, InSb, ZnSe, and CdTe, however, the GGA gives no consistent improvement over the LSDA. The lattice parameters are underestimated significantly (0.3–3 %) by the LSDA, whereas the GGA values are within 1% deviation from experiment. In contrast to this improvement over the LSDA, the GGA error becomes larger for the bulk moduli; the LSDA error is -10–10 %, while the GGA error is -20 to 10 %. It is noted that the GGA always lengthens the lattice parameters and reduces the bulk moduli, compared with the LSDA results, and therefore that the GGA gives worse results if the LSDA results are in good agreement with the experimental results.

Finally we have discussed the accuracy of the perturbative treatment for the GC effect. According to the Hohenberg-Kohn theorem, there exists a unique energy functional which is a variational in the spin density. Therefore, if the GGA spin-density functional is evaluated with a trial spin density close to the exact ground-state density, the error in the total energy is only of second order. Based on this idea, we have shown that accurate GGA total energies can be obtained with LSDA spin densities, thus avoiding the self-consistency iterations for the GGA functional. Moreover, we have discussed that a full spin-density scheme with spherical potentials yields for the considered systems the same accuracy for the total energy as a full-potential calculation.

The KKR Green's-function method will be more and more useful for the study of electronic and atomic structures

of complex systems, such as impurities, surface, and disordered alloys, because it has been very accurate, as shown in the present paper, and because it is easily extended, with the same accuracy as that of the bulk calculations, to nonperiodic systems.[7]

ACKNOWLEDGMENT

This work was partially supported by a Grant-in-Aid for Scientific Research on Priority Area from the Ministry of Education, Science, Sports and Culture of Japan.

[1] J. Korringa, Physica (Amsterdam) **13**, 392 (1947).
[2] W. Kohn and N. Rostoker, Phys. Rev. **94**, 1111 (1954).
[3] O. K. Andersen, Phys. Rev. B **12**, 3060 (1975).
[4] D. D. Koelling and G. O. Arbman, J. Phys. F **5**, 2041 (1975).
[5] P. H. Dederichs, B. Drittler, and R. Zeller, in *Application of Multiple Scattering Theory to Material Science*, edited by W. H. Butler, P. H. Dederichs, A. Gonis, and R. L. Weaver, MRS Symposia Proceedings No. 253 (Material Research Society, Pittsburgh, 1992), p. 185.
[6] R. Zeller, P. Lang, B. Drittler, and P. H. Dederichs, in *Application of Multiple Scattering Theory to Material Science* (Ref. 5), p. 357.
[7] I. Turek, V. Drchal, J. Kudrnovský, M. Šob, and P. Weinberger, *Electronic Structure of Disordered Alloys, Surfaces and Interfaces* (Kluwer Academic, Dordrecht, 1997).
[8] W. H. Butler, in *Application of Multiple Scattering Theory to Material Science* (Ref. 5), p. 149.
[9] B. Dritter, M. Weinert, R. Zeller, and P. H. Dederichs, Solid State Commun. **79**, 31 (1991).
[10] N. Papanikolaou, R. Zeller, P. H. Dederichs, and N. Stefanou, Phys. Rev. B **55**, 4157 (1997).
[11] N. Papanikolaou, R. Zeller, P. H. Dederichs, and N. Stefanou, Comput. Mater. Sci. **8**, 131 (1997).
[12] D. M. Nicholson and J. S. Faukner, Phys. Rev. B **39**, 8187 (1989).
[13] W. H. Butler, A. Gonis, and X.-G. Zhang, Phys. Rev. B **45**, 11 527 (1992).
[14] S. Bei der Kellen, Yoonsik Oh, E. Badralexe, and A. J. Freeman, Phys. Rev. B **51**, 9560 (1995).
[15] T. Huhne, C. Zecha, H. Ebert, P. H. Dederichs, and R. Zeller, Phys. Rev. B **58**, 10 236 (1998).
[16] P. Hohenberg and W. Kohn, Phys. Rev. **136**, B864 (1964).
[17] W. Kohn and L. J. Sham, Phys. Rev. **140**, A1133 (1965).
[18] L. Hedin and B. I. Lundqvist, J. Phys. C **4**, 2064 (1971).
[19] V. von Barth and L. Hedin, J. Phys. C **5**, 1629 (1972).
[20] V. L. Morruzi, J. F. Janak, and A. R. Williams, *Calculated Electronic Properties of Metals* (Pergamon, New York, 1978).
[21] S. H. Vosko, L. Wilk, and M. Nusair, Can. J. Phys. **58**, 1200 (1980).
[22] J. P. Perdew, in *Electronic Structure of Solids '91*, edited by P. Ziesche and H. Eschrig (Academie Verlag, Berlin, 1991), p. 11.
[23] J. P. Perdew, J. A. Chevary, S. H. Vosko, K. A. Jackson, M. R. Pederson, D. J. Singh, and C. Fiolhais, Phys. Rev. B **46**, 6671 (1992).
[24] V. Ozolinš and M. Körling, Phys. Rev. B **48**, 18 304 (1993).
[25] L. Vitos, J. Kollár, and H. L. Skriver, Phys. Rev. B **49**, 16 694 (1994).
[26] L. Vitos, J. Kollár, and H. L. Skriver, Phys. Rev. B **55**, 13 521 (1997).
[27] R. Zeller, J. Phys. C **20**, 2347 (1987).
[28] R. Zeller, M. Asato, T. Hoshino, J. Zabloudil, P. Weinberger, and P. H. Dederichs, Philos. Mag. B **78**, 417 (1998).
[29] N. Stefanou, H. Akai, and R. Zeller, Comput. Phys. Commun. **60**, 231 (1990).
[30] N. Stefanou and R. Zeller, J. Phys.: Condens. Matter **3**, 7599 (1991).
[31] R. Zeller, J. P. Deutz, and P. H. Dederichs, Solid State Commun. **44**, 993 (1982).
[32] K. Wildberger, P. Lang, R. Zeller, and P. H. Dederichs, Phys. Rev. B **52**, 11 502 (1995).
[33] S. Blügel, H. Akai, R. Zeller, and P. H. Dederichs, Phys. Rev. B **35**, 3271 (1987).
[34] The different MT prescriptions mainly affect the treatment of the atomiclike core states, which we confine within the MT volume. In fixed-MT calculations, the volume does not change and the confinement error is insensitive to the change of the lattice parameter. In scaled-MT calculations, the MT volume changes and the confinement error becomes different for different lattice parameters.
[35] C. Kittel, *Introduction to Solid State Physics*, 5th ed. (Wiley, New York, 1976).
[36] F. D. Murnagham, Proc. Natl. Acad. Sci. USA **30**, 244 (1944).
[37] D. J. Singh, W. E. Pickett, and H. Krakauer, Phys. Rev. B **43**, 11 628 (1991).
[38] K. B. Hathaway, H. J. Jansen, and A. J. Freeman, Phys. Rev. B **31**, 7603 (1985).
[39] C. Filippi, D. J. Singh, and C. J. Umrigar, Phys. Rev. B **50**, 14 947 (1994).
[40] *Landolt-Börnstein, New Series*, Vol. 22, edited by O. Madelung (Springer-Verlag, Berlin, 1987).
[41] Preliminary results for the perturbative treatment are already discussed by T. Hoshino, M. Asato, T. Asada, R. Zeller, and P. H. Dederichs, J. Magn. Magn. Mater. **177-181**, 1411 (1998).
[42] The present ASA-KKR calculations overestimate *a* and underestimate *B* for Fe, compared with the FP-KKR results (see Sec. III), which are very similar to the FP-LMTO results, while they underestimate *a* and overestimate *B* for Al, Ni, Cu, Rh, Pd, and Ag, compared with the FP-KKR results. Contrary to the present ASA-KKR results, the LMTO-ASA calculations by Körling and Häglund [Phys. Rev. B **45**, 13 293 (1992)] overestimate *a* and underestimate *B* for Ni, Cu, Rh, Pd, and Ag, compared with the FP-LMTO results (Ref. 24). Dr. Timo Korhonen recalculated *a* and *B* for Pd, using his LMTO-ASA program, and obtained results similar to the present ASA-KKR results but different from the results of Körling and Häglund.
[43] B. Drittler, M. Weinert, R. Zeller, and P. H. Dederichs, Phys. Rev. B **39**, 930 (1989).
[44] P. H. Dederichs, T. Hoshino, B. Drittler, K. Abraham, and R. Zeller, Physica B **172**, 203 (1991).
[45] B. Drittler, M. Weinert, R. Zeller, and P. H. Dederichs, Phys. Rev. B **42**, 9336 (1990).